IEEE Photonics Journal
An IEEE Photonics Society Publication

Open Access

Ka-Band Tunable Flat-Top Microwave Photonic Filter Using a Multi-Phase-Shifted Fiber Bragg Grating

Volume 6, Number 4, August 2014

Ye Deng
Ming Li, Member, IEEE
Ningbo Huang
Ninghua Zhu, Member, IEEE

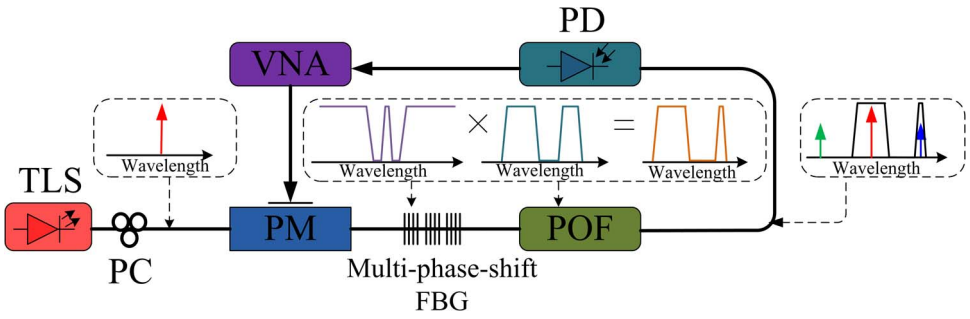

DOI: 10.1109/JPHOT.2014.2339327
1943-0655

Ka-Band Tunable Flat-Top Microwave Photonic Filter Using a Multi-Phase-Shifted Fiber Bragg Grating

Ye Deng, Ming Li, *Member, IEEE*, Ningbo Huang, and Ninghua Zhu, *Member, IEEE*

Institute of Semiconductors, Chinese Academy of Sciences, Beijing 100083, China

DOI: 10.1109/JPHOT.2014.2339327

Manuscript received June 9, 2014; revised July 3, 2014; accepted July 9, 2014. Date of current version July 25, 2014. This work was supported by the National Natural Science Foundation of China under Grants 61377002, 61321063, and 61090391. The work of M. Li was supported in part by the "Thousand Young Talent" program. Corresponding author: M. Li (e-mail: ml@semi.ac.cn).

Abstract: A tunable single-bandpass microwave photonic filter (MPF) with a narrow and flat-top shape operating in high frequency range is proposed and experimentally demonstrated, using a specially designed multi-phase-shift fiber Bragg grating (FBG) cascaded with a programmable optical filter (POF). The key device in the proposed MPF is the multi-phase-shift FBG, providing a flat-top passband with a narrow 3-dB bandwidth of 813 MHz in transmission. Consequently, in the MPF, a single passband with a 3- and 20-dB bandwidths of 840 MHz and 2.43 GHz is achieved, respectively. Moreover, an operating frequency range from 27.1 to 38.1 GHz is realized by tuning the wavelength of the optical carrier and adjusting the transfer function of the POF. To the best of our knowledge, this proposed filter provides the highest tunable frequency coverage in Ka-band ever reported for MPFs with a single narrow and flat-top passband.

Index Terms: Fiber Bragg gratings, modulation, micro-optics, frequency filtering.

1. Introduction

Microwave photonic filters (MPFs) have attracted considerable interests in the past few years, thanks to the advantageous features such as large frequency coverage, flexible tunability, light weight and immunity to electromagnetic interference [1]–[5]. Therefore, for many applications in wireless communication, modern radar and electronic warfare systems, MPFs are highly desired for processing broadband and high frequency microwave signals, comparable to conventional electrical filters [6]. One typical technique for realizing MPFs is the use of multi-tap optical delay line structure or channelization [7]–[9]. In [9], due to the nature of the discrete time signal processing, multiple harmonic passbands are achieved with a Gaussian-like spectral response. In addition, although high sidelobe suppression ratio could be achieved, it can only work at a low frequency due to the dispersion-induced power fading effect. As we know, the realization of a single-bandpass MPF at higher frequency is required in many important microwave/millimeter-wave signal processing applications. Recently, MPFs with a single passband have been demonstrated, by using a Mach-Zehnder interferometer [10], a ring resonator [11], or stimulated Brillouin scattering (SBS) in a nonlinear fiber [12], [13]. Although a single passband was obtained in [10]–[13], the profile of the passband is not as flat as expected. Recently, a flat-top MPF was proposed by using phase modulation together with a pair of fiber Bragg gratings (FBGs) [14].

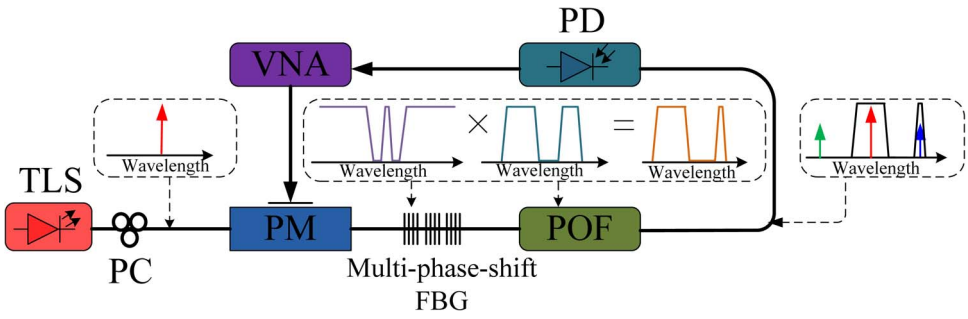

Fig. 1. Schematic of the proposed MPF. TLS: tunable laser source, PC: polarization controller, PM: phase modulator, POF: programmable optical filter, PD: photodetector, VNA: vector network analyzer.

Due to the large bandwidth of the used FBGs, the 3-dB bandwidth is as large as 2 GHz. A flat-top MPF with a 1.5 GHz bandwidth was obtained based on an optical comb source [15]. By using an optical pulse shaper to control each comb line, the passband is reconfigurable. However, the system is complicated and the 3-dB bandwidth of the MPF is also wide. In addition, a tunable MPF with an ultranarrow and flat-top passband based on phase-modulation to intensity-modulation (PM-IM) conversion and a specific superstructure FBG (SFBG) was demonstrated [16], with a 3-dB and a 20-dB bandwidths of 170 and 372 MHz achieved, respectively. However, the tunable range of the center frequency only ranges from 0.4 GHz to 6.4 GHz, due to the limited reflection bandwidth of the SFBG and the notch location within the reflection band. Here, we are aiming at the realization of an MPF with a single narrow passband ($<$ 1 GHz), flat-top shape, and tunable high-frequency coverage.

In this paper, we propose and experimentally demonstrate a tunable single-bandpass MPF with narrow and flat-top shape operating in high frequency range, in particular in Ka-band (27–40 GHz [17]). By using a specially designed multi-phase-shift FBG cascaded with a programmable optical filter (POF), an MPF with a 3-dB and a 20-dB bandwidths of 840 MHz and 2.43 GHz is designed, respectively. By tuning the wavelength of the optical carrier and adjusting the transfer function of the POF, a tunable frequency coverage from 27.1 GHz to 38.1 GHz is obtained. This is the highest tunable frequency coverage ever reported for the MPF with a narrow, flat-top and single passband frequency response, to the best of our knowledge. Note that, the tunable frequency coverage of the proposed MPF can be further extended by increasing the bandwidth of the phase modulator (PM) and the photodetector (PD).

2. Principle

The proposed MPF is schematically shown in Fig. 1, consisting of a tunable laser source (TLS), a polarization controller (PC), a PM, a multi-phase-shift FBG, a POF and a PD. In the proposed MPF, a continuous wave (CW) lightwave from the TLS is sent to the PM via the PC. The polarization state of the light wave is adjusted by the PC to minimize the polarization-dependent loss. Within the PM, the CW lightwave is modulated by a sinusoidal microwave signal generated by a vector network analyzer (VNA). At the output of the PM, the phase modulated optical signal is sent to the multi-phase-shift FBG and the POF. The multi-phase-shift FBG is a special FBG which is fabricated by introducing two π-phase shifts into the refractive index modulation profile. Here, each π-phase shift produces a Lorentz-shaped passband in the stopband and the combination of the two Lorentz-shaped passbands results in a passband with a narrow and flat top [16]. Then, the POF is employed to select the narrow flat-top passband and a part of transmission spectrum of the multi-phase-shift FBG. Therefore, the combination of the specific FBG and the POF act as a dual-channel optical filter with a wide passband and a narrow flat-top passband. The optical carrier is centered at the wide passband and the narrow flat-top passband is located far from the optical carrier by a frequency spacing corresponding to the center

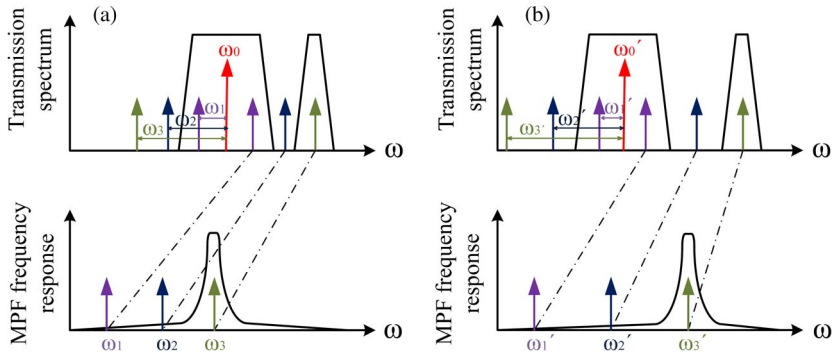

Fig. 2. Transmission spectrum of the multi-phase-shift FBG cascaded with the POF and frequency response of the MPF at different optical carrier: (a) $\omega_c = \omega_0$; (b) $\omega_c = \omega_0'$.

frequency of the MPF. It is noted that the wide passband should be symmetrical around the optical carrier.

More details regarding the operation principle of the proposed MPF is shown in Fig. 2(a). For low-frequency signal at ω_1, both the first order sidebands of the modulated optical signal fall within the wide passband. The beating signal between the optical carrier ω_0 and the $+1$st order sideband cancels completely the beating one between the optical carrier and the -1st order sideband because the two signals are out of phase. Hence, no microwave signal appears at the output of the PD. As the signal frequency increases gradually, a microwave signal will occur, once the $+1$st order sideband $(\omega_0 + \omega_3)$ falls within the narrow flat-top passband and the -1st order sideband $(\omega_0 - \omega_3)$ locates outside the wide passband. Using the VNA, a narrow flat-top passband will be observed in the MPF frequency response. More importantly, thanks to the large frequency spacing between the wide passband and the narrow flat-top passband, an operation at high-frequency (e.g., Ka-band) band is ensured. Additionally, as shown in Fig. 2(b), by tuning the wavelength of the optical carrier and adjusting the transfer function of the POF, a tunable high-frequency coverage is achieved.

Mathematically, the optical field at the PM under small-signal modulation is described as [18]

$$\begin{aligned} E_{PM}(t) &= E_0 \exp[j\omega_0 t + j\beta cos(\omega_m t + \Phi_m)] \\ &\approx E_0 J_0(\beta) \exp(j\omega_0 t) + E_0 J_1(\beta) \exp[j(\omega_0 t + \omega_m t + \Phi_m + \pi/2)] \\ &\quad - E_0 J_1(\beta) \exp[j(\omega_0 t - \omega_m t - \Phi_m - \pi/2)] \end{aligned} \tag{1}$$

where E_0 is the optical field of the lightwave from the TLS, ω_0 and ω_m are the angular frequency of the lightwave and the microwave signal respectively, $J_n(\cdot)$ is the n th-order Bessel function of the first kind where $n = 0, \pm 1$, β is the phase modulation index, and Φ_m is the initial phase of the microwave signal.

The designed multi-phase-shift FBG is divided into N grating sections which can be considered as a cascade of $N-1$ equivalent cavities with coupling effects among them [19]. According to the transfer matrix method [20], the amplitude responses of the multi-phase-shift FBG can be expressed as

$$\begin{aligned} \begin{bmatrix} A_f(0) \\ A_b(0) \end{bmatrix} &= \begin{bmatrix} F_{11} & F_{12} \\ F_{21} & F_{22} \end{bmatrix} \times \begin{bmatrix} A_f(L) \\ A_b(L) \end{bmatrix} \\ &= \prod_{i=1}^{N-1} \begin{bmatrix} F_{11}^i & F_{12}^i \\ F_{21}^i & F_{22}^i \end{bmatrix} \times \begin{bmatrix} \exp(j\theta_i/2) & 0 \\ 0 & \exp(-j\theta_i/2) \end{bmatrix} \times \begin{bmatrix} F_{11}^N & F_{12}^N \\ F_{21}^N & F_{22}^N \end{bmatrix} \times \begin{bmatrix} A_f(L) \\ A_b(L) \end{bmatrix} \end{aligned} \tag{2}$$

where $A_f(z)$ and $A_b(z)$ are the amplitude of the optical signal propagating forward and backward along the grating fiber, L is the length of the multi-phase-shift FBG, and θ_i represents the ith

phase shift (in particular, $\theta_i = \pi$). The 2 $\times$ 2 matrix F^i denotes the amplitude response corresponding to the ith grating section. Its elements are given by [21]

$$F_{11}^i = \left(F_{22}^i\right)^* = \cosh(SL_i) - j(\widehat{\sigma}/S)\sinh(SL_i) \tag{3}$$

$$F_{12}^i = \left(F_{21}^i\right)^* = -j(\kappa/S)\sinh(SL_i) \tag{4}$$

where $*$ represents complex conjugation, L_i is the length of ith grating section, $S = \sqrt{\kappa^2 - \widehat{\sigma}^2}$, κ is the "ac" coupling coefficient and $\widehat{\sigma}$ is the general "dc" self-coupling coefficient.

According to the coupled-mode theory [22] and the transfer matrix method [20], the amplitude transmission coefficient $t(\omega)$, the power transmission coefficient $T(\omega)$ and the phase response $\theta(\omega)$ of the multi-phase-shift FBG can be calculated as

$$t(\omega) = A_f(L)/A_f(0) = 1/F_{11} \tag{5}$$

$$T(\omega) = |t(\omega)|^2 \tag{6}$$

$$\theta(\omega) = phase[t(\omega)]. \tag{7}$$

The phase-modulated optical signal propagates through the multi-phase-shift FBG and the POF. When one sideband (assuming the +1st order sideband) is located in the narrow flat-top passband, the corresponding optical field at the output of the POF can be expressed as

$$E_{out}(t) = \sqrt{T(\omega_0)T'(\omega_0)}E_0J_0(\beta)\exp[j\omega_0 t + j\theta(\omega_0) + j\theta'(\omega_0)] + \sqrt{T(\omega_0+\omega_m)T'(\omega_0+\omega_m)} \times E_0J_1(\beta)\exp[j(\omega_0 t + \omega_m t + \Phi_m + \pi/2) + j\theta(\omega_0+\omega_m) + j\theta'(\omega_0+\omega_m)], \tag{8}$$

where $T'(\omega)$ and $\theta'(\omega)$ denote the power transmission response and the phase response of the POF.

Through PM-IM conversion, a microwave signal is generated and sent to the VNA for frequency response measurement. The output microwave signal $V(\omega_m)$ and its power $P(\omega_m)$ are described as

$$V(\omega_m) \propto ac\left\{|E_{out}(t)|^2\right\} \approx 2E_0^2J_0(\beta)J_1(\beta)Acos[\omega_m t + \Phi_m + \pi/2 + \Delta\theta] \tag{9}$$

$$P(\omega_m) = |V(\omega_m)|^2 = 4E_0^4A^2J_0^2(\beta)J_1^2(\beta) \tag{10}$$

where

$$A = \sqrt{T(\omega_0)T'(\omega_0)T(\omega_0+\omega_m)T'(\omega_0+\omega_m)} \tag{11}$$

$$\Delta\theta = \theta(\omega_0+\omega_m) + \theta'(\omega_0+\omega_m) - \theta(\omega_0) - \theta'(\omega_0) \tag{12}$$

and $ac(\cdot)$ represents the "ac" term of the output electrical signal.

Therefore, it can be seen from (9) and (10) that the phase-modulated optical signal is converted a microwave signal in the PD. Therefore, through PM-IM conversion, a desired frequency response that reflects the shape of the narrow flat-top passband of the multi-phase-shift FBG is achieved for the proposed MPF. At the mean time, the key significance of the proposed MPF lies in its high-frequency operation range. The lower limit of the frequency coverage is determined by the stopband bandwidth of the multi-phase-shift FBG and the narrow flat-top passband location within the stopband. The upper limit of the frequency coverage is affected by the bandwidths of the used PM and PD, which can be further extended by increasing these devices' bandwidths.

3. Experiments

In this section, experiments are carried out based on the scheme shown in Fig. 1. The multi-phase-shift FBG used is fabricated in a standard single-mode fiber by using ultraviolet beam scanning and the motion of a uniform-period phase mask [19]. The key important steps for

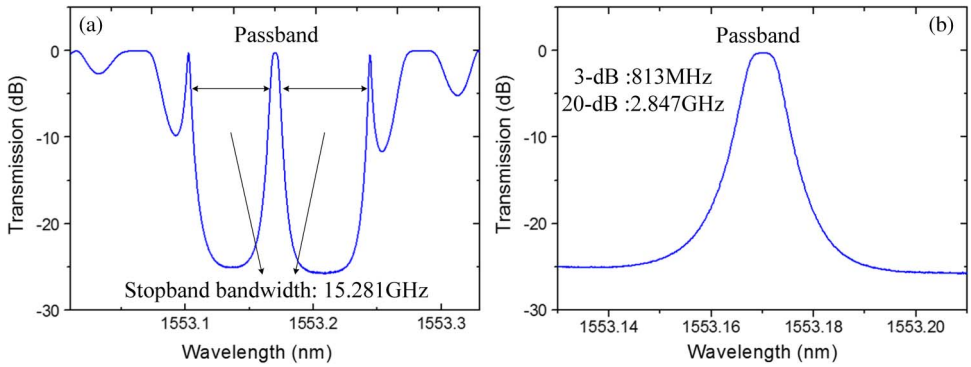

Fig. 3. (a) Transmission spectrum of the multi-phase-shift FBG. (b) Zoom-in view of the transmission spectrum of the passband.

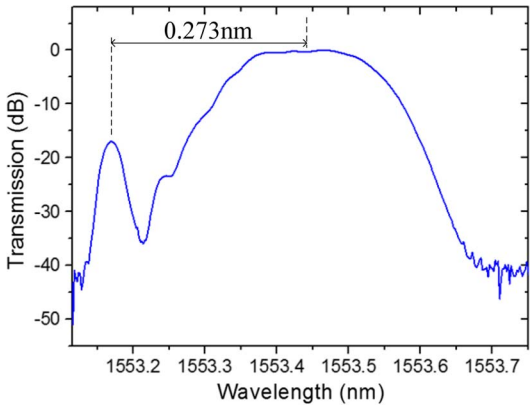

Fig. 4. Transmission spectrum of the combination of the multi-phase-shift FBG and the POF.

fabrication are the implementations of the Gaussian apodization and the phase shifts. Through controlling the scanning speed of the ultraviolet beam along the fiber, the Gaussian apodization in refractive index perturbation is formed. Two phase shifts are formed along the 32-mm FBG with a maximum index modulation of 2.9×10^{-4}. The measured transmission spectrum with a stopband bandwidth of 15.281 GHz is shown in Fig. 3(a). The insertion loss at the transmission peak is measured to be nearly 0.3 dB. A zoom-in view over the narrow transmission window is obtained in Fig. 3(b), as a tunable laser (Agilent 8164A) with its wavelength scanning by steps of 0.1 pm is used. It is obvious that, a narrow, flat-top passband at 1553.17 nm is achieved with a 3-dB bandwidth of 813 MHz and a 20-dB bandwidth of 2.847 GHz.

A TLS (Agilent 8164B) with linewidth less than 100 kHz is used as the optical source and a VNA (Agilent 8722ET) is employed. To measure the frequency response of the MPF, a sinusoidal microwave signal from the VNA is applied to the PM, with the output frequency sweeping from 50 MHz to 40 GHz. The power level of the microwave signal is fixed as -5 dBm. A POF (Finisar 4000S) with minimum filter bandwidth of 10 GHz is employed to reshape the transmission spectrum of the multi-phase-shift FBG. The resulting transmission spectrum of the combination of the multi-phase-shift FBG and the POF is shown in Fig. 4. The wide passband is centered at 1553.443 nm and a frequency spacing of 0.273 nm (i.e., 34 GHz) between the wide passband and the narrow one is generated. It can be seen that there is nearly 18 dB difference on the suppression ratio of transmission spectrum between narrow flat-top passband and the wide passband. Due to the limited resolution of the optical spectrum analyzer (OSA), the magnitude of the narrow flat-top passband can not be precisely shown. Note that, the difference on the suppression ratio of transmission spectrum between narrow flat-top passband and the wide

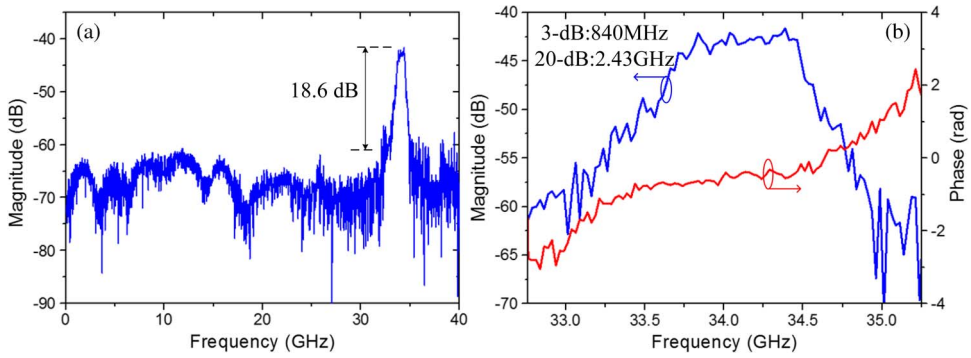

Fig. 5. (a) Measured transmission response of the proposed MPF. (b) Zoom-in view of the magnitude and the phase responses with the center frequency tuned at 34.1 GHz.

passband may affect the performance of the MPF. It is because that the microwave signal sent back to the VNA is generated by beating the optical carrier and the −1st order sideband. If the sideband suppression ratio of the narrow flat-top passband is higher, the suppression ration of the MPF will also accordingly become higher.

A lightwave at 1553.443 nm from the TLS with fixed power 10 mW is then sent to the PM via the PC. When the microwave frequency is equal to the frequency spacing between the optical carrier and the center of the narrow flat-top passband, the −1st order sideband will be located in the passband of the multi-phase-shift FBG while the +1st order sideband will be filtered out. The −1st order sideband and the optical carrier are directed to the PD with a 3-dB bandwidth of 40 GHz. Through PM-IM conversion, a microwave signal at the output of the PD is generated and it is then sent back to the VNA for frequency response measurement.

Fig. 5 shows the measured frequency response of the proposed MPF. It is clearly seen that there is a single passband with a narrow bandwidth and a flat-top shape. The center frequency of the single passband is at 34.1 GHz which is just equal to the frequency spacing between the optical carrier and the narrow flat-top passband of the multi-phase-shift FBG. In detail, the flatness of the passband is estimated to be less than ±0.98 dB, and the 3-dB and the 20-dB bandwidths are 840 MHz and 2.43 GHz respectively, showing a good agreement with the transmission spectrum of the multi-phase-shift FBG. Here, a shape factor which is defined as the ratio between the 20-dB and the 3-dB bandwidths is calculated to be 2.89. In addition, the ratio of the transmission peak to the sidelobe is 18.6 dB. This ratio can be increased by adjusting the POF to make a more symmetrical characteristic of the wide passband, since the PM-IM conversion at the wide passband would convert the asymmetric amplitude response to noise. It can be seen that the measured microwave photonic filter response suffers from some noise. Ripples in both magnitude and phase response are observed in Fig. 5. The ripples in the filtering response maybe result from the external environment-induced phase fluctuation between the optical carrier and the −1st order sideband. In addition, the magnitude and phase fluctuations of the multi-phase-shift FBG's spectral response will also be transferred into the ripples of the MPF.

Next, the tunability of the center frequency of the MPF is achieved by tuning the wavelength of the optical carrier and adjusting the transfer function of the POF. As shown in Fig. 6, the tunable center frequency of the passband covers a range from 27.1 to 38.1 GHz. It is worth noting that the tunable frequency coverage here is greatly limited by the bandwidth of the PM and the PD. Thus the tunable frequency coverage can be further extended by employing a PM and a PD with a wider bandwidth. The total insertion loss of the MPF is about 40 dB. The large insertion loss mainly results from the large loss of the POF and the low optical-electrical conversion efficiency of the PD. By using an electrical amplifier (EA), the loss can be greatly compensated. The measured variation of the 3-dB bandwidth of the MPF over the tuning range is within 70 MHz as the result of the magnitude and phase response ripples of the multi-phase-shift FBG.

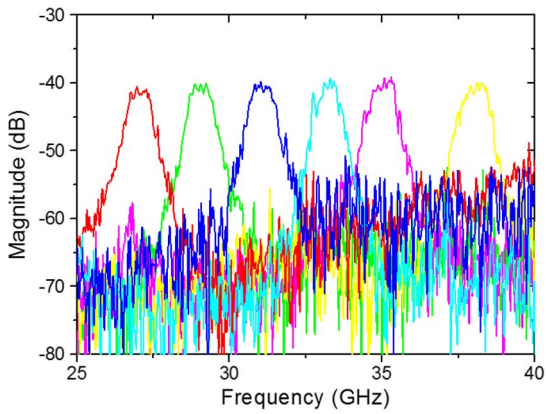

Fig. 6. Measured frequency response of the proposed MPF with the center frequency tuned from 27.1 GHz to 38.1 GHz.

The spurious free dynamic range (SFDR) of our proposed Ka-band MPF is also measured, which is about 50 dB $\cdot$ $Hz^{2/3}$. Note that, the central frequency tunability is achieved by manually tuning the wavelength of the optical carrier and adjusting the transfer function of the POF, the tuning speed of the proposed MPF is not fast.

4. Conclusion

A tunable single-bandpass MPF with a narrow and flat-top shape operating in high-frequency range (i.e., Ka-band) was proposed and experimentally demonstrated. In the proposed MPF, the multi-phase-shift FBG with a 3-dB and 20-dB bandwidths of 840 MHz and 2.43 GHz was fabricated to generate a narrow, flat-top passband in the optical domain. Aided with the POF providing a wide passband, a single narrow, flat-top passband with a 3-dB and 20-dB bandwidths of 840 MHz and 2.43 GHz was achieved in the proposed MPF. Furthermore, the MPF is characterized by its operation in high frequency range, i.e. Ka-band. Also, the operation frequency can be tuned to cover a range from 27.1 GHz to 38.1 GHz. By increasing the bandwidth of the PM and the PD, the tunable frequency coverage of the proposed MPF can be extended further.

References

[1] J. Capmany, B. Ortega, and D. Pastor, "A tutorial on microwave photonic filters," *J. Lightw. Technol.*, vol. 24, no. 1, pp. 201–229, Jan. 2006.
[2] J. Yao, "Microwave photonics," *J. Lightw. Technol.*, vol. 27, no. 3, pp. 314–335, Feb. 2009.
[3] J. Capmany and D. Novak, "Microwave photonics combines two worlds," *Nat. Photon.*, vol. 1, pp. 319–330, 2007.
[4] A. J. Seeds, "Microwave photonics," *IEEE Trans. Microw. Theory Tech.*, vol. 50, no. 3, pp. 877–887, Mar. 2002.
[5] J. Capmany *et al.*, "Microwave photonic signal processing," *J. Lightw. Technol.*, vol. 31, no. 4, pp. 571–586, Feb. 2013.
[6] J. Marti and A. Griol, "Harmonic suppressed microstrip multistage coupled ring bandpass filters," *Electron. Lett.*, vol. 34, no. 2, pp. 2140–2142, Oct. 1998.
[7] R. A. Minasian, "Photonic signal processing of microwave signals," *IEEE Trans. Microw. Theory Tech.*, vol. 54, no. 2, pp. 832–846, Feb. 2006.
[8] X. Zou, W. Li, W. Pan, L. Yan, and J. Yao, "Photonic-assisted microwave channelizer with improved channel characteristics based on spectrum-controlled stimulated Brillouin scattering," *IEEE Trans. Microw. Theory Tech.*, vol. 61, no. 9, pp. 3470–3478, Sep. 2013.
[9] J. S. Leng, W. Zhang, and J. A. R. Williams, "Optimization of superstructured fiber Bragg gratings for microwave photonic filters response, " *IEEE Photon. Technol. Lett.*, vol. 16, no. 7, pp. 1736–1738, Jul. 2004.
[10] J. Mora *et al.*, "Photonic microwave tunable single-bandpass filter based on a Mach-Zehnder interferometer," *J. Lightw. Technol.*, vol. 24, no. 7, pp. 2500–2509, Jul. 2006.
[11] J. Palací, G. E. Villanueva, J. V. Galán, J. Martí, and B. Vidal, "Single bandpass photonic microwave filter based on a notch ring resonator, " *IEEE Photon. Technol. Lett.*, vol. 22, no. 17, pp. 1276–1278, Sep. 2010.
[12] W. Zhang and R. A. Minasian, "Widely tunable single-passband microwave photonic filter based on stimulated Brillouin scattering," *IEEE Photon. Technol. Lett.*, vol. 23, no. 23, pp. 1775–1777, Dec. 2011.

[13] Y. M. Chang and J. H. Lee, "High-Q tunable, photonic microwave single passband filter based on stimulated Brillouin scattering and fiber Bragg grating filtering," *Opt. Commun*., vol. 281, no. 20, pp. 5146–5151, Oct. 2008.
[14] X. Yi and R. A. Minasian, "Microwave photonic filter with single bandpass response," *Electron. Lett*., vol. 45, no. 7, pp. 362–363, Mar. 2009.
[15] M. Song *et al*., "Reconfigurable and tunable flat-top microwave photonic filters utilizing optical frequency comb," *IEEE Photon. Technol. Lett*., vol. 23, no. 21, pp. 1618–1620, Nov. 2011.
[16] L. Gao, X. Chen, and J. Yao, "Tunable microwave photonic filter with a narrow and flat-top passband," *IEEE Microw. Wireless Compon. Lett*., vol. 23, no. 7, pp. 362–364, Jul. 2013.
[17] *IEEE Standard Letter Designations for Radar-Frequency Bands*, IEEE Std. 521–1984, 1984.
[18] G. Qi, J. P. Yao, J. Seregelyi, C. Bélisle, and S. Paquet, "Optical generation and distribution of continuously tunable millimeter-wave signals using an optical phase modulator," *J. Lightw. Technol*., vol. 23, no. 9, pp. 2687–2695, Sep. 2005.
[19] X. Zou *et al*., "All-fiber optical filter with an ultranarrow and rectangular spectral response," *Opt. Lett*., vol. 38, no. 16, pp. 3096–3098, Aug. 2013.
[20] G. P. Agrawal and S. Radic, "Phase-shifted fiber Bragg grating and their application for wavelength demultiplexing, " *IEEE Photon. Technol. Lett*., vol. 6, no. 8, pp. 995–997, Aug. 1994.
[21] T. Erdogan, "Fiber grating spectra," *J. Lightw. Technol*., vol. 15, no. 8, pp. 277–1294, Aug. 1997.
[22] H. A. Haus and W. Huang, "Coupled-mode theory," *Proc. IEEE*, vol. 79, no. 10, pp. 1505–1518, Oct. 1991.